

Structure and metallicity of phase V of hydrogen

Bartomeu Monserrat,^{1,2,*} Neil D. Drummond,³ Philip Dalladay-Simpson,⁴ Ross T. Howie,⁴
Pablo López Ríos,^{2,5} Eugene Gregoryanz,^{4,6,7} Chris J. Pickard,^{8,9} and Richard J. Needs²

¹*Department of Physics and Astronomy, Rutgers University, Piscataway, New Jersey 08854-8019, USA*

²*TCM Group, Cavendish Laboratory, University of Cambridge,
J. J. Thomson Avenue, Cambridge CB3 0HE, United Kingdom*

³*Department of Physics, Lancaster University, Lancaster LA1 4YB, United Kingdom*

⁴*Center for High Pressure Science and Technology Advanced Research, Shanghai, People's Republic of China*

⁵*Max-Planck Institute for Solid State Research, Heisenbergstraße 1, 70569 Stuttgart, Germany*

⁶*Centre for Science at Extreme Conditions and School of Physics and Astronomy,
University of Edinburgh, Edinburgh EH9 3JZ, United Kingdom*

⁷*Key Laboratory of Materials Physics, Institute of Solid State Physics,
Chinese Academy of Sciences, Hefei, People's Republic of China*

⁸*Department of Materials Science and Metallurgy, University of Cambridge,
27 Charles Babbage Road, Cambridge CB3 0FS, United Kingdom*

⁹*Advanced Institute for Materials Research, Tohoku University 2-1-1 Katahira, Aoba, Sendai, 980-8577, Japan*

(Dated: June 11, 2018)

A new phase V of hydrogen was recently claimed in experiments above 325 GPa and 300 K. Due to the extremely small sample size at such record pressures the measurements were limited to Raman spectroscopy. The experimental data on increase of pressure shows decreasing Raman activity and darkening of the sample, which suggests band-gap closure and impending molecular dissociation, but no definite conclusions could be reached. Furthermore, the available data is insufficient to determine the structure of phase V, which remains unknown. Introducing saddle-point *ab initio* random structure searching (sp-AIRSS), we find several new structural candidates of hydrogen which could describe the observed properties of phase V. We investigate hydrogen metallisation in the proposed candidate structures, and demonstrate that smaller band gaps are associated with longer bond lengths. We conclude that phase V is a stepping stone towards metallisation.

The study of dense hydrogen is important to fundamental physics and astrophysics [1–4]. Currently the most interesting question relates to the metallisation and dissociation of molecular hydrogen under pressure, which has not yet been achieved in the solid state, even though it was first proposed in 1935 [5]. The known phases I, II, III, and IV/IV' of solid hydrogen, which have been characterised extensively experimentally [6–10] and theoretically [11–19], exhibit molecular bonds and are insulating.

Dalladay-Simpson and co-workers recently reported Raman spectroscopy experiments on H₂, D₂, and HD up to pressures of 388 GPa at 300 K [20]. In these experiments, they identified a new phase V of H₂ and HD above 325 GPa and at 300 K, which was suggested to be at the onset of dissociation and could therefore represent a stepping stone towards full metallisation. Several experimental reports followed, claiming metallisation of H₂ under different pressure-temperature conditions [21, 22], but the validity of these experiments is yet to be confirmed [23, 24]. In this Letter, we focus on phases IV, IV', and V as described in Refs. [10, 20].

On the theoretical front, a number of candidate structures have been proposed to explain the observed experimental phases of high-pressure hydrogen up to 300 GPa [11, 13, 14, 25]. Of these, the monoclinic *C2/c* structure is currently the best candidate for phase III around 300 GPa [11, 25], as it exhibits Raman and infrared (IR) spectra consistent with those observed experi-

mentally. The monoclinic *Pc* structure is the best candidate for phase IV [13, 14] due to its mixed layered nature that leads to the two vibron peaks observed experimentally. Recent quantum Monte Carlo and free energy calculations have confirmed these phases to be energetically favourable in the pressure range in which phases III and IV are observed [19]. The most stable atomic hydrogen candidate structure is tetragonal and has space group *I4₁/amd* [11, 12, 17, 18]. Despite the large number of candidate structures known for high-pressure hydrogen, none provides a good model for the recent experimental observations at pressures above about 300 GPa.

Discovering candidate structures using searching methods has been successful in many systems, particularly at high pressure [26–30]. As an example, the lowest-enthalpy candidate structures for phases II, III, and IV of hydrogen have been found using the *ab initio* random structure searching (AIRSS) method [11, 13, 14]. The experimental discovery of phase V, for which there is no obvious candidate structure, prompts the question of whether it is necessary to go beyond current structure searching methods in this case.

Standard structure searching methods such as AIRSS are restricted to structures associated with minima of the potential energy landscape. However, thermodynamically stable structures associated with saddle points that are dynamically stabilised by anharmonic nuclear motion are known to exist [31, 32]. The high-temperature cubic

perovskite phase of BaTiO₃ provides a well-known example [31, 33].

A variety of computational methods has been used to determine the dynamical stability of such structures, including Monte Carlo [33], molecular dynamics [34, 35], path integral molecular dynamics [36, 37], and local anharmonic vibrational methods [38–42]. These methods can determine the dynamical stability of a known saddle-point structure but they have not been used to find previously unknown saddle-point structures. The following question arises: can we devise a systematic approach to searching for previously unknown structures associated with saddle points of the energy landscape? The large nuclear effects of hydrogen make it an ideal system in which to explore this possibility.

We address these questions using saddle-point *ab initio* random structure searching (sp-AIRSS). Saddle-point structures stabilised by anharmonic nuclear motion are typically of higher symmetry than their *broken-symmetry* counterparts. Based on this observation, we use sp-AIRSS to impose high-symmetry constraints during structure searches. For example, imposing cubic symmetry on BaTiO₃, leads to the known cubic phase, but removing the symmetry constraints leads instead to the rhombohedral phase. The symmetry constraints bias the search towards the high-symmetry structures that are expected to be stable when the vibrational amplitudes are large. We emphasise that this strategy enables the discovery of structures which cannot be found in unconstrained searches because correspond to minima of the free energy landscape but not of the static lattice energy landscape. We then remove the symmetry constraints and relax the reference structure using an anharmonic vibrational method. In this work we have used the vibrational self-consistent field method of Ref. [41], but any of the available anharmonic methods may be applicable at this stage of the calculation [33–42]. The structure may then relax to a minimum or saddle point of the potential energy landscape.

The lowest-enthalpy known hydrogen structures have monoclinic symmetry with space groups $C2/c$ (model for phase III) and Pc (model for phase IV) [11, 13, 14]. To search for new candidate structures we have therefore performed sp-AIRSS searches imposing space groups of orthorhombic or higher symmetry. The searches have led to the discovery of three new energetically competitive structures at pressures for which phase V is observed. These structures have orthorhombic symmetry with space groups $Pca2_1$, $Pna2_1$, and $Pcaa$, and 48 atoms in the primitive cell. $Pca2_1$ and $Pna2_1$ are mixed layered structures similar to Pc in which alternate layers exhibit shorter and longer molecular bond lengths, resulting in two vibron peaks in the Raman and IR spectra. $Pcaa$ has a single type of layer.

Our analysis in this work is based on these three new structures, together with the previously reported struc-

tures $C2/c$ [11], $Cmca-4$ and $Cmca-12$ [11] (where 4 and 12 indicate the number of atoms in the primitive cell), Pc [13, 14] and $Ibam$ [11]. The $C2/c$ and $Cmca$ structures model phase III and all theoretical methods predict that $C2/c$ is more stable at lower pressures and $Cmca$ at higher pressures, but the precise pressure above which $Cmca$ becomes stable is highly-dependent on the level of theory used. A hexagonal structure of space group $P6_122$ has recently been proposed as a candidate for phase III at pressures below 200 GPa [25], but in this work we focus on higher pressures, and therefore do not include it in our analysis. The $Ibam$ structure is an extreme member of the family of mixed structures, in which the weakly-bound layer is graphene-like and molecular bonds are no longer present.

Of all structures considered, $Pna2_1$ and $Pca2_1$ are dynamically unstable at the harmonic vibrational level, and their broken-symmetry counterpart is a monoclinic structure. $Ibam$ is also dynamically unstable, while the rest are dynamically stable. Note that unless sp-AIRSS had been used, $Pca2_1$ and $Pna2_1$ would have fallen into the corresponding broken-symmetry monoclinic structure, and would have gone unnoticed. The symmetry constraints prevent this and allow the potential discovery of new structures stabilised by anharmonic vibrations.

We have used first-principles methods based on density functional theory (DFT) as implemented in the CASTEP [43] code to calculate the relative stability of the eight structures under consideration. We have used both the BLYP exchange-correlation functional [44, 45], which has been shown to be accurate for the description of molecular hydrogen structures [46], and the PBE exchange-correlation functional [47], which we find to favour atomic phases compared to the BLYP functional. Due to the small energy differences between competing structures of only a few meV, the resulting phase diagrams are sensitive to the level of theory used [19, 46, 48]. We therefore also perform selected diffusion Monte Carlo (DMC) calculations using the CASINO package [49] to establish the validity of our conclusions based on the DFT results. To calculate the vibrational contribution to the energy including anharmonic contributions we use the method of Refs. [41, 50]. Further details of the first principles calculations are provided in the Supplemental Material [51].

In Figs. 1a and 1b we report static lattice enthalpies, zero-temperature enthalpies (including quantum zero-point motion), and Gibbs free energies at 300 K relative to $C2/c$ using DFT. The static lattice enthalpies of $Pca2_1$, $Pna2_1$, and $Ibam$ are shown as dashed lines to indicate dynamical instability at the harmonic level corresponding to saddle points of the potential energy landscape. All three structures become dynamically stable when lattice vibrations are included. We also show selected static lattice DMC calculations in Fig. 1c.

For both BLYP and PBE calculations, we observe that

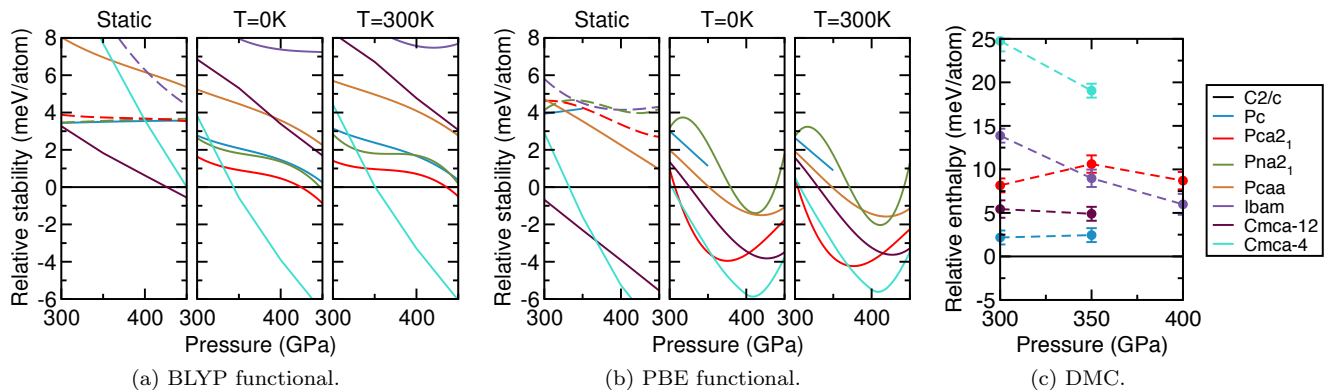


FIG. 1. Relative enthalpies using the (a) BLYP and (b) PBE DFT functionals, and using (c) DMC. The DFT results are at the static lattice level, at $T = 0$ K (including zero-point motion), and at $T = 300$ K, and the dashed lines in the static lattice diagrams indicate enthalpies corresponding to structures at saddle-points of the energy landscape. The DMC results are at the static lattice level, and the dashed lines between the DMC points are a guide to the eye only.

the *Cmca-4* structure is the lowest in energy at the higher pressures studied. This is consistent with earlier DFT studies, but we note that using more accurate DMC calculations de-stabilises this structure and removes it from the phase diagram (see Fig. 1c). The *Cmca-12* structure is also de-stabilised within DMC, although to a smaller degree than the *Cmca-4* structure.

The BLYP results show that, of the mixed layered structures, *Pca2₁* is the most competitive energetically at both zero and 300 K, becoming more stable than *C2/c* at pressures of about 420 GPa. The PBE results also favour *Pca2₁* as the most stable mixed layered structure, but it becomes more stable than *C2/c* at significantly lower pressures of about 300 GPa, consistently with the observation that PBE favours atomic phases compared to molecular phases (*Pca2₁* has alternate layers with longer bond lengths than those observed in *C2/c*). We also note that, at the PBE level, *Pc* does not exist above about 375 GPa, as it falls into the *Cmca-4* structure. Finally, we note that the *Pcaa* structure, which is not energetically competitive at the BLYP level, becomes more competitive at the PBE level, a fact that we again attribute to the longer bond lengths exhibited by *Pcaa* when compared to *C2/c*. Our static DMC calculations combined by the DFT vibrational energy estimates confirm that *Pca2₁* remains energetically competitive as a candidate structure of high pressure hydrogen (see Supplemental Material [51]).

The experimental Raman spectrum of phase V is compared to the theoretical harmonic spectra of *Pc* and *Pca2₁* calculated using the PBE functional in Fig. S4. Figure 2a shows a comparison of the Raman intensities at 374 GPa. In the high-frequency regime, the frequency of the experimental ν_2 vibron agrees with those of *Pc* and *Pca2₁*. The frequency of the ν_1 vibron is marginally better reproduced by *Pc* than by *Pca2₁*. We also note that Magdău and Ackland showed that anharmonic contribu-

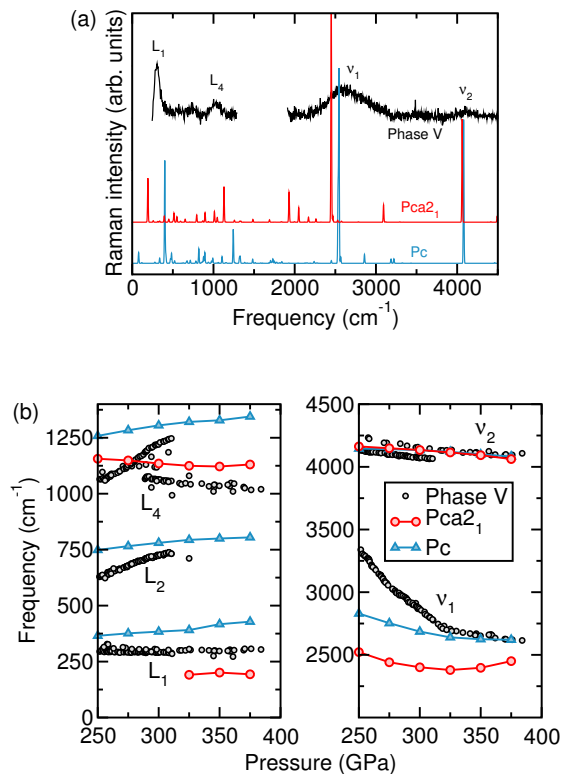


FIG. 2. (a) Raman spectra of *Pc*, *Pca2₁*, and phase V at 374 GPa. The absence of data in the range 1500–1900 cm^{-1} arises from the strong signal from the diamonds at these frequencies. (b) Pressure dependence of the frequencies of the most intense Raman peaks of *Pc*, *Pca2₁*, and phase V.

tions push the ν_2 vibron to higher energies in *Pc* [16], and a similar behaviour in *Pca2₁* would bring the latter into better agreement with experiment. At the low-frequency regime the L_1 and L_4 modes of phase V are in better agreement with *Pca2₁* than with *Pc*. The L_2 mode,

which disappears upon entering phase V, is present in Pc but missing in $Pca2_1$.

The pressure dependence of the Raman peaks is shown in Fig. 2b, with phase IV below 325 GPa, and phase V at higher pressures. The pressure dependence of the ν_2 vibron is well-reproduced by both Pc and $Pca2_1$. The frequency of the low-energy vibron has a pressure dependence of $-1.4 \text{ cm}^{-1}/\text{GPa}$ in phase V above 325 GPa, which is much weaker than that of phase IV at lower pressures (note the change in slope for ν_1 around 325 GPa). The pressure dependence of ν_1 in Pc and $Pca2_1$ is too weak at pressures below 325 GPa, suggesting that they are not good candidates for phase IV. However, we note that, as discussed earlier, anharmonic effects significantly affect this frequency [16], and therefore we cannot discard these structures as candidates for phase IV. The pressure dependence of the low frequency part of the Raman spectrum of phase V is better-reproduced by $Pca2_1$ than by Pc .

A striking feature of the experimental Raman spectrum is the dramatic increase in the width of the L_1 peak upon entering phase V, whose FWHM increases from about 70 cm^{-1} at 325 GPa to about 160 cm^{-1} at 388 GPa. The experimental data show that the increase in the peak width is strongly isotope dependent [20], suggesting a nuclear origin for this feature. Therefore, it could be attributed to a harmonic dynamical instability like the one exhibited by the $Pca2_1$ and $Pna2_1$ structures.

Our Raman spectra analysis suggests that the $Pca2_1$ structure is consistent with phase V. The Raman spectrum of $Pna2_1$ is almost identical to that of Pc , and both give poorer agreement with experiment than $Pca2_1$. The $C2/c$, $Cmca$, and $Pcaa$ structures cannot describe phase V, as they have a unique type of bond and thus a single vibron. $Ibam$ is also an unlikely candidate for phase V, as its vibron ν_1 has a frequency below 2250 cm^{-1} in the pressure range where phase V is observed. Details of the Raman spectra of these phases are provided in the Supplemental Material [51].

Overall, $Pca2_1$ is energetically competitive at the pressures at which phase V has been observed, and crucially, of all structures considered, only its Raman spectrum is consistent with that of phase V. More generally, the known Pc structure and the new $Pna2_1$ and $Pca2_1$ structures are plausible candidates for the high pressure hydrogen structures characterised by two strong vibrons, that is, phases IV, IV', and V.

Having discovered good candidate structures, we study the metallicity of phase V. The study of band gap closure and metallisation in high pressure hydrogen is a challenging problem. Band gaps are typically underestimated by several electronvolts by Kohn-Sham DFT [52, 53], whereas the neglect of electron-phonon coupling contributions tends to lead to an overestimation of the gap size [54, 55]. These two effects alter the gap in oppo-

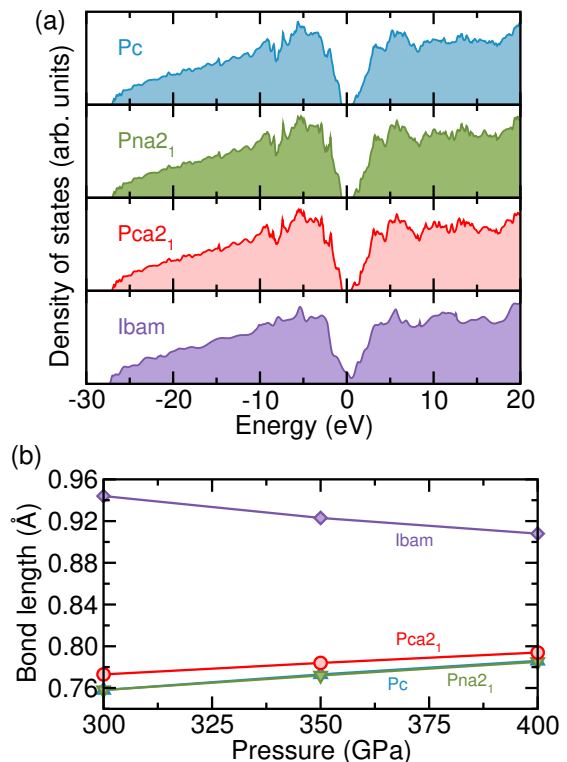


FIG. 3. (a) Electronic densities of states of hydrogen candidate mixed layered structures Pc , $Pna2_1$, $Pca2_1$, and $Ibam$ at a pressure of 350 GPa. (b) Static bond lengths of the Pc , $Pna2_1$, $Pca2_1$, and $Ibam$ structures for the layers with longer bonds. The bond lengths of Pc and $Pna2_1$ are indistinguishable.

site directions, cancelling to some extent. We consider static lattice DFT band structures, which contain valuable insights on trends amongst the different structures, but cannot be used reliably to estimate the actual band gap values.

Metallisation in layered hydrogen structures has been proposed to arise from the weakly bound layers that can be described as distorted graphene sheets [56]. Here, we extend this analysis to mixed-layered structures, where layers with short and long bond lengths coexist. In Fig. 3a we show the electronic densities of states at 350 GPa for the four mixed layered structures considered in this work. Pc , $Pna2_1$, and $Pca2_1$ are all insulating. Of these four structures, $Pca2_1$ has the smallest band gap by about 0.3 eV. This is a consequence of the longer bond length in the weakly bound layers, as shown in Fig. 3b. The bond lengths of all of these structures in the strongly-bound layers are comparable.

Molecular dissociation is more pronounced in $Ibam$, as the weakly bound layers are graphene-like, and the molecular character is lost. This is shown by the longer bond lengths exhibited by $Ibam$ in the graphene sheets (Fig. 3b). The frequency of the ν_1 vibron in $Ibam$ in-

creases with pressure, as expected from the decreasing bond length of the graphene sheets. In contrast, the increase in bond length with pressure in Pc , $Pna2_1$, and $Pca2_1$ indicates that the pressure dependence of the ν_1 vibron in these structures is qualitatively different from that of $Ibam$, and consistent with the experimental observation of phase V. $Ibam$ might become stable at higher pressures, although our DFT calculations do not support this conjecture.

For completeness, we emphasize that at 0 K, the metallic atomic $I4_1/amd$ structure is predicted to become thermodynamically stable at a pressure of around 400 GPa [17, 18]. It would be interesting to assess the relative stability of $I4_1/amd$ with respect to the mixed structures around room temperature, but this is beyond the scope of the present work.

Overall, our energetic and spectroscopic results show that $Pca2_1$ is a promising model structure for hydrogen phase V. It exhibits longer bond lengths compared to those of other similar structures, suggesting that phase V is a stepping stone towards the metallisation of hydrogen.

B.M. acknowledges support from the Winton Programme for the Physics of Sustainability, and from Robinson College, Cambridge, and the Cambridge Philosophical Society for a Henslow Research Fellowship. E.G. and R.J.N. acknowledge financial support from the Engineering and Physical Sciences Research Council (EPSRC) of the United Kingdom (Grants No. EP/J003999/1 and No. EP/P034616/1, respectively). C.J.P. is supported by the Royal Society through a Royal Society Wolfson Research Merit award. The calculations were performed on the Darwin Supercomputer of the University of Cambridge High Performance Computing Service facility (<http://www.hpc.cam.ac.uk/>), the Archer facility of the UK national high performance computing service, for which access was obtained via the UKCP consortium and funded by EPSRC grant No. EP/P022596/1, and the Oak Ridge Leadership Computing Facility at the Oak Ridge National Laboratory, which is supported by the Office of Science of the US Department of Energy under Contract No. DE-AC05-00OR22725.

* bm418@cam.ac.uk

- [1] N. W. Ashcroft, “Metallic hydrogen: A high-temperature superconductor?” *Phys. Rev. Lett.* **21**, 1748–1749 (1968).
- [2] Isaac F. Silvera, “The solid molecular hydrogens in the condensed phase: Fundamentals and static properties,” *Rev. Mod. Phys.* **52**, 393–452 (1980).
- [3] Jeffrey M. McMahon, Miguel A. Morales, Carlo Pierleoni, and David M. Ceperley, “The properties of hydrogen and helium under extreme conditions,” *Rev. Mod. Phys.* **84**, 1607–1653 (2012).
- [4] Alexander F. Goncharov, Ross T. Howie, and Eugene Gregoryanz, “Hydrogen at extreme pressures,” *Low Temp. Phys.* **39**, 402–408 (2013).
- [5] E. Wigner and H. B. Huntington, “On the possibility of a metallic modification of hydrogen,” *J. Chem. Phys.* **3**, 764–770 (1935).
- [6] Isaac F. Silvera and Rinke J. Wijngaarden, “New low-temperature phase of molecular deuterium at ultrahigh pressure,” *Phys. Rev. Lett.* **47**, 39–42 (1981).
- [7] R. J. Hemley and H. K. Mao, “Phase transition in solid molecular hydrogen at ultrahigh pressures,” *Phys. Rev. Lett.* **61**, 857–860 (1988).
- [8] M. I. Eremets and I. A. Troyan, “Conductive dense hydrogen,” *Nat. Mater.* **10**, 927 (2011).
- [9] Ross T. Howie, Christophe L. Guillaume, Thomas Scheler, Alexander F. Goncharov, and Eugene Gregoryanz, “Mixed molecular and atomic phase of dense hydrogen,” *Phys. Rev. Lett.* **108**, 125501 (2012).
- [10] Ross T. Howie, Thomas Scheler, Christophe L. Guillaume, and Eugene Gregoryanz, “Proton tunneling in phase IV of hydrogen and deuterium,” *Phys. Rev. B* **86**, 214104 (2012).
- [11] Chris J. Pickard and Richard J. Needs, “Structure of phase III of solid hydrogen,” *Nat. Phys.* **3**, 473–476 (2007).
- [12] Jeffrey M. McMahon and David M. Ceperley, “High-temperature superconductivity in atomic metallic hydrogen,” *Phys. Rev. B* **84**, 144515 (2011).
- [13] Chris J. Pickard, Miguel Martinez-Canales, and Richard J. Needs, “Density functional theory study of phase IV of solid hydrogen,” *Phys. Rev. B* **85**, 214114 (2012).
- [14] Chris J. Pickard, Miguel Martinez-Canales, and Richard J. Needs, “Erratum: Density functional theory study of phase IV of solid hydrogen [Phys. Rev. B **85**, 214114 (2012)],” *Phys. Rev. B* **86**, 059902(E) (2012).
- [15] Hanyu Liu, Li Zhu, Wenwen Cui, and Yanming Ma, “Room-temperature structures of solid hydrogen at high pressures,” *J. Chem. Phys.* **137**, 074501 (2012).
- [16] Ioan B. Magdău and Graeme J. Ackland, “Identification of high-pressure phases III and IV in hydrogen: Simulating Raman spectra using molecular dynamics,” *Phys. Rev. B* **87**, 174110 (2013).
- [17] Sam Azadi, Bartomeu Monserrat, W. M. C. Foulkes, and R. J. Needs, “Dissociation of high-pressure solid molecular hydrogen: A quantum Monte Carlo and anharmonic vibrational study,” *Phys. Rev. Lett.* **112**, 165501 (2014).
- [18] Jeremy McMinis, Raymond C. Clay, Donghwa Lee, and Miguel A. Morales, “Molecular to atomic phase transition in hydrogen under high pressure,” *Phys. Rev. Lett.* **114**, 105305 (2015).
- [19] N. D. Drummond, B. Monserrat, J. H. Lloyd-Williams, P. López Ríos, C. J. Pickard, and R. J. Needs, “Quantum Monte Carlo study of the phase diagram of solid molecular hydrogen at extreme pressures,” *Nat. Commun.* **6**, 7794 (2015).
- [20] Philip Dalladay-Simpson, Ross T. Howie, and Eugene Gregoryanz, “Evidence for a new phase of dense hydrogen above 325 gigapascals,” *Nature* **529**, 63 (2016).
- [21] Ranga P. Dias and Isaac F. Silvera, “Observation of the Wigner-Huntington transition to metallic hydrogen,” *Science* **355**, 715–718 (2017).
- [22] M. I. Eremets, A. P. Drozdov, P. P. Kong, and H. Wang, “Molecular semimetallic hydrogen,” [arXiv:1708.05217](https://arxiv.org/abs/1708.05217) (2017).

- [23] Xiao-Di Liu, Philip Dalladay-Simpson, Ross T. Howie, Bing Li, and Eugene Gregoryanz, “Comment on “Observation of the Wigner-Huntington transition to metallic hydrogen,”” *Science* **357**, eaan2286 (2017).
- [24] Alexander F. Goncharov and Viktor V. Struzhkin, “Comment on “Observation of the Wigner-Huntington transition to metallic hydrogen,”” *Science* **357**, eaam9736 (2017).
- [25] Bartomeu Monserrat, Richard J. Needs, Eugene Gregoryanz, and Chris J. Pickard, “Hexagonal structure of phase III of solid hydrogen,” *Phys. Rev. B* **94**, 134101 (2016).
- [26] Chris J. Pickard and R. J. Needs, “High-pressure phases of silane,” *Phys. Rev. Lett.* **97**, 045504 (2006).
- [27] Artem R. Oganov and Colin W. Glass, “Crystal structure prediction using *ab initio* evolutionary techniques: Principles and applications,” *J. Chem. Phys.* **124**, 244704 (2006).
- [28] Yanchao Wang, Jian Lv, Li Zhu, and Yanming Ma, “Crystal structure prediction via particle-swarm optimization,” *Phys. Rev. B* **82**, 094116 (2010).
- [29] Chris J. Pickard and R. J. Needs, “*Ab initio* random structure searching,” *J. Phys. Condens. Matter* **23**, 053201 (2011).
- [30] David C. Lonie and Eva Zurek, “Xtalopt: An open-source evolutionary algorithm for crystal structure prediction,” *Comput. Phys. Commun.* **182**, 372–387 (2011).
- [31] M. E. Lines and A. M. Glass, *Principles and Applications of Ferroelectrics and Related Materials* (Oxford University Press, 2001).
- [32] Göran Grimvall, Blanka Magyari-Köpe, Vidvuds Ozoliņš, and Kristin A. Persson, “Lattice instabilities in metallic elements,” *Rev. Mod. Phys.* **84**, 945–986 (2012).
- [33] W. Zhong, David Vanderbilt, and K. M. Rabe, “Phase transitions in BaTiO₃ from first principles,” *Phys. Rev. Lett.* **73**, 1861–1864 (1994).
- [34] B. J. Alder and T. E. Wainwright, “Studies in molecular dynamics. I. General method,” *J. Chem. Phys.* **31**, 459–466 (1959).
- [35] R. Car and M. Parrinello, “Unified approach for molecular dynamics and density-functional theory,” *Phys. Rev. Lett.* **55**, 2471–2474 (1985).
- [36] Jianshu Cao and Gregory A. Voth, “The formulation of quantum statistical mechanics based on the Feynman path centroid density. I. Equilibrium properties,” *J. Chem. Phys.* **100**, 5093–5105 (1994).
- [37] Jianshu Cao and Gregory A. Voth, “The formulation of quantum statistical mechanics based on the Feynman path centroid density. II. Dynamical properties,” *J. Chem. Phys.* **100**, 5106–5117 (1994).
- [38] P. Souvatzis, O. Eriksson, M. I. Katsnelson, and S. P. Rudin, “Entropy driven stabilization of energetically unstable crystal structures explained from first principles theory,” *Phys. Rev. Lett.* **100**, 095901 (2008).
- [39] O. Hellman, I. A. Abrikosov, and S. I. Simak, “Lattice dynamics of anharmonic solids from first principles,” *Phys. Rev. B* **84**, 180301 (2011).
- [40] Nikolas Antolin, Oscar D. Restrepo, and Wolfgang Windl, “Fast free-energy calculations for unstable high-temperature phases,” *Phys. Rev. B* **86**, 054119 (2012).
- [41] Bartomeu Monserrat, N. D. Drummond, and R. J. Needs, “Anharmonic vibrational properties in periodic systems: Energy, electron-phonon coupling, and stress,” *Phys. Rev. B* **87**, 144302 (2013).
- [42] Ion Errea, Matteo Calandra, and Francesco Mauri, “Anharmonic free energies and phonon dispersions from the stochastic self-consistent harmonic approximation: Application to platinum and palladium hydrides,” *Phys. Rev. B* **89**, 064302 (2014).
- [43] Stewart J. Clark, Matthew D. Segall, Chris J. Pickard, Phil J. Hasnip, Matt I. J. Probert, Keith Refson, and Mike C. Payne, “First principles methods using CASTEP,” *Z. Kristallogr.* **220**, 567 (2005).
- [44] A. D. Becke, “Density-functional exchange-energy approximation with correct asymptotic behavior,” *Phys. Rev. A* **38**, 3098–3100 (1988).
- [45] Chengteh Lee, Weitao Yang, and Robert G. Parr, “Development of the Colle-Salvetti correlation-energy formula into a functional of the electron density,” *Phys. Rev. B* **37**, 785–789 (1988).
- [46] Raymond C. Clay, Jeremy Mcminis, Jeffrey M. McMahon, Carlo Pierleoni, David M. Ceperley, and Miguel A. Morales, “Benchmarking exchange-correlation functionals for hydrogen at high pressures using quantum Monte Carlo,” *Phys. Rev. B* **89**, 184106 (2014).
- [47] John P. Perdew, Kieron Burke, and Matthias Ernzerhof, “Generalized gradient approximation made simple,” *Phys. Rev. Lett.* **77**, 3865 (1996).
- [48] Sam Azadi and W. M. C. Foulkes, “Fate of density functional theory in the study of high-pressure solid hydrogen,” *Phys. Rev. B* **88**, 014115 (2013).
- [49] R. J. Needs, M. D. Towler, N. D. Drummond, and P. López Ríos, “Continuum variational and diffusion quantum Monte Carlo calculations,” *J. Phys. Condens. Matter* **22**, 023201 (2010).
- [50] Jonathan H. Lloyd-Williams and Bartomeu Monserrat, “Lattice dynamics and electron-phonon coupling calculations using nondiagonal supercells,” *Phys. Rev. B* **92**, 184301 (2015).
- [51] See Supplemental Material at [...] for numerical details of the sp-AIRSS searches, of the anharmonic vibrational calculations, of the quantum Monte Carlo calculations, of the Raman spectra of candidate structures, and cif files for the *Pca*₂₁, *Pna*₂₁, and *Pcaa* structures relaxed within PBE at 350 GPa. It includes Refs. [57–62].
- [52] Sam Azadi, W. M. C. Foulkes, and Thomas D. Kühne, “Quantum Monte Carlo study of high pressure solid molecular hydrogen,” *New J. Phys.* **15**, 113005 (2013).
- [53] Sam Azadi, N. D. Drummond, and W. M. C. Foulkes, “Nature of the metallization transition in solid hydrogen,” *Phys. Rev. B* **95**, 035142 (2017).
- [54] Miguel A. Morales, Jeffrey M. McMahon, Carlo Pierleoni, and David M. Ceperley, “Towards a predictive first-principles description of solid molecular hydrogen with density functional theory,” *Phys. Rev. B* **87**, 184107 (2013).
- [55] Sam Azadi, Ranber Singh, and Thomas D. Kühne, “Nuclear quantum effects induce metallization of dense solid molecular hydrogen,” *J. Comput. Chem.* **39**, 262 (2018).
- [56] R. E. Cohen, Ivan I. Naumov, and Russell J. Hemley, “Electronic excitations and metallization of dense solid hydrogen,” *Proc. Natl. Acad. Sci. USA* **110**, 13757–13762 (2013).
- [57] David Vanderbilt, “Soft self-consistent pseudopotentials in a generalized eigenvalue formalism,” *Phys. Rev. B* **41**, 7892–7895 (1990).
- [58] Joon O. Jung and R. Benny Gerber, “Vibrational wave functions and spectroscopy of (H₂O)_n, n = 2, 3, 4, 5:

- Vibrational self-consistent field with correlation corrections,” *J. Chem. Phys.* **105**, 10332–10348 (1996).
- [59] Joel M. Bowman, “Self-consistent field energies and wavefunctions for coupled oscillators,” *J. Chem. Phys.* **68**, 608–610 (1978).
- [60] W. M. C. Foulkes, L. Mitas, R. J. Needs, and G. Rajagopal, “Quantum Monte Carlo simulations of solids,” *Rev. Mod. Phys.* **73**, 33–83 (2001).
- [61] C. Lin, F. H. Zong, and D. M. Ceperley, “Twist-averaged boundary conditions in continuum quantum Monte Carlo algorithms,” *Phys. Rev. E* **64**, 016702 (2001).
- [62] Hendra Kwee, Shiwei Zhang, and Henry Krakauer, “Finite-size correction in many-body electronic structure calculations,” *Phys. Rev. Lett.* **100**, 126404 (2008).

Supplemental Material for “Structure and metallicity of phase V of hydrogen”

COMPUTATIONAL DETAILS OF STRUCTURE SEARCHES

The structure searches have been performed using the sp-AIRSS method introduced in this work. The best candidates known so far for phases III and IV of hydrogen are monoclinic structures, and therefore our sp-AIRSS searches have focused on higher-symmetry structures, starting with orthorhombic crystal systems.

Searches have been performed for simulation cells containing up to 96 atoms, at pressures of 100, 120, 150, 200, 300, 350, 450, 500, and 600 GPa. The electronic energies were evaluated using the density functional theory (DFT) plane-wave pseudopotential code CASTEP [S43] (version 7) with default “on the fly” ultrasoft pseudopotentials [S57] and the BLYP [S44, S45] and PBE [S47] density functionals. Energy cut-offs of 230 eV, and Monkhorst-Pack \mathbf{k} -point grids of spacing $2\pi \times 0.07 \text{ \AA}^{-1}$ have been used for the searches. The total number of structures generated by the sp-AIRSS calculations was 45,344.

COMPUTATIONAL DETAILS OF ANHARMONIC CALCULATIONS

The sp-AIRSS calculations found several new structures with low static lattice enthalpies. These have been further investigated using the vibrational self-consistent field method described in Ref. [S41]. These calculations consist of two steps: (i) a mapping of the Born-Oppenheimer (BO) energy surface beyond the local harmonic region, and (ii) the solution of the resulting vibrational Schrödinger equation using a mean-field ansatz and second order perturbation theory.

The sampling of the BO energy surface follows the principal axes approximation (PAA) [S41, S58]:

$$\epsilon_{\text{PAA}}(\mathbf{u}) = \epsilon(\mathbf{0}) + \sum_{\mathbf{q},\nu} V_{\mathbf{q}\nu}(u_{\mathbf{q}\nu}) + \frac{1}{2} \sum_{\mathbf{q},\nu} \sum_{\mathbf{q}',\nu'}' V_{\mathbf{q}\nu;\mathbf{q}'\nu'}(u_{\mathbf{q}\nu}, u_{\mathbf{q}'\nu'}) + \dots, \quad (\text{S1})$$

where $u_{\mathbf{q}\nu}$ is the amplitude of a normal mode coordinate at the vibrational Brillouin zone point \mathbf{q} and branch index ν , and \mathbf{u} is a vector including the amplitudes of all normal mode coordinates in the system. The 1-body terms $V_{\mathbf{q}\nu}$ are allowed to have a dependence on $u_{\mathbf{q}\nu}$ beyond that of the harmonic approximation, and the 2-body terms provide additional anharmonic corrections arising from the 2-dimensional subspaces that they span. The mapping has been performed with DFT, using the CASTEP code [S43] (version 7) with default “on the fly” ultrasoft pseudopotentials [S57] and the BLYP [S44, S45] and PBE [S47] functionals. We also exploited the recently introduced non-diagonal supercells method which allows us to obtain results that are converged with respect to the simulation cell size [S50]. The computational parameters for the final calculations reported in the main text consist of an energy cut-off of 1000 eV and Monkhorst-Pack \mathbf{k} -point grids of spacing $2\pi \times 0.025 \text{ \AA}^{-1}$. These parameters allow us to obtain differences between frozen-phonon structures that are converged to better than 10^{-4} eV/atom for the energy, forces to better than 10^{-4} eV/Å, and stresses to better than 10^{-3} GPa. The anharmonic mapping of the BO energy surface is performed along the directions determined by the normal modes of vibration, with maximum amplitudes of $5\sqrt{\langle u^2 \rangle}$, and converged results are obtained by sampling 17 points along each direction. The resulting energy data is fitted using cubic splines, which provide more accurate fits than polynomial expansions for the strongly anharmonic hydrogen systems studied here. We note that this differs from the approach used originally in Ref. [S41], in which polynomials were used to fit the anharmonic BO energy surface.

In Fig. S1 we show a 2-dimensional subspace of the BO energy surface of $Pca2_1$. The subspace is spanned by two normal modes, u_1 and u_2 , for which the corresponding harmonic frequencies are imaginary $\omega_1^2, \omega_2^2 < 0$. Figure S1a shows the approximate 2-dimensional subspace when only 1-body anharmonic terms are considered in the expansion of the BO energy surface, while Fig. S1b shows the corresponding subspace with the inclusion of 2-body terms. The inclusion of 2-body terms raises the vibrational energy, therefore contributing to the stabilisation of the structure. The inclusion of 2-body terms affects the energies of the structures, but does not modify their nature (whether they are dynamically stable or not.)

The resulting Schrödinger equation is solved using a mean-field ansatz by writing the wave function as a Hartree product, obtaining the vibrational self-consistent field equations that have been used previously in molecules and

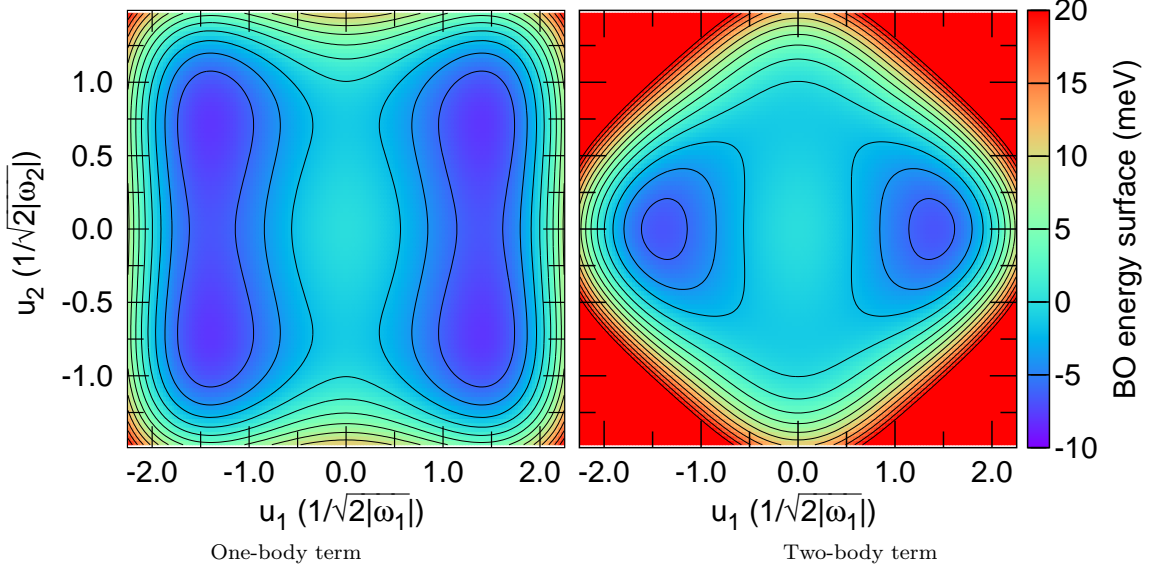


FIG. S1. 2-dimensional subspace spanned by two unstable modes within (a) the mapping of the BO energy surface along the two 1-dimensional lines $(u_1, 0)$ and $(0, u_2)$, and (b) the exact mapping of the BO energy surface in the 2-dimensional plane (u_1, u_2) . The results are for the $Pca2_1$ structure at $P = 300$ GPa.

solids [S41, S59]:

$$\left(-\frac{1}{2}\frac{\partial^2}{\partial u_{\mathbf{q}\nu}^2} + \bar{V}_{\mathbf{q}\nu}(u_{\mathbf{q}\nu})\right) |\phi_{\mathbf{q}\nu}(u_{\mathbf{q}\nu})\rangle = \lambda_{\mathbf{q}\nu} |\phi_{\mathbf{q}\nu}(u_{\mathbf{q}\nu})\rangle, \quad (\text{S2})$$

$$\bar{V}_{\mathbf{q}\nu}(u_{\mathbf{q}\nu}) = \left\langle \prod_{\mathbf{q}', \nu'} \phi_{\mathbf{q}'\nu'}(u_{\mathbf{q}'\nu'}) \left| \epsilon_{\text{PAA}}(\mathbf{u}) \right| \prod_{\mathbf{q}', \nu'} \phi_{\mathbf{q}'\nu'}(u_{\mathbf{q}'\nu'}) \right\rangle. \quad (\text{S3})$$

The final energy is

$$E = \sum_{\mathbf{q}, \nu} \lambda_{\mathbf{q}\nu} + \left\langle \prod_{\mathbf{q}, \nu} \phi_{\mathbf{q}\nu}(u_{\mathbf{q}\nu}) \left| \epsilon_{\text{PAA}}(\mathbf{u}) - \sum_{\mathbf{q}, \nu} \bar{V}_{\mathbf{q}, \nu}(u_{\mathbf{q}\nu}) \right| \prod_{\mathbf{q}, \nu} \phi_{\mathbf{q}\nu}(u_{\mathbf{q}\nu}) \right\rangle. \quad (\text{S4})$$

The second order perturbative correction to the energy in state \mathbf{S} is given by [S41]:

$$E_{\text{vib}, \mathbf{S}}^{(2)} = \sum_{\mathbf{S}' \neq \mathbf{S}} \frac{1}{E_{\mathbf{S}} - E_{\mathbf{S}'}} \left| \left\langle \prod_{\mathbf{q}, \nu} \phi_{\mathbf{q}\nu}^{S'} \left| \epsilon_{\text{PAA}}(\mathbf{u}) - \sum_{\mathbf{q}, \nu} \bar{V}_{\mathbf{q}\nu}(u_{\mathbf{q}\nu}) \right| \prod_{\mathbf{q}, \nu} \phi_{\mathbf{q}\nu}^{\mathbf{S}} \right\rangle \right|^2. \quad (\text{S5})$$

These energies are then used to calculate the anharmonic free energy \mathcal{F} at finite temperature T according to [S41]:

$$\mathcal{F} = -\frac{1}{\beta} \ln \mathcal{Z}, \quad (\text{S6})$$

where $\beta = 1/k_{\text{B}}T$ is the inverse temperature, k_{B} is Boltzmann's constant, and $\mathcal{Z} = \sum_{\mathbf{S}} e^{-\beta E_{\mathbf{S}}}$ is the partition function, calculated as a sum over vibrational states \mathbf{S} of anharmonic energy $E_{\mathbf{S}}$.

We expand the anharmonic wave function associated with each degree of freedom, $|\phi_{\mathbf{q}\nu}(u_{\mathbf{q}\nu})\rangle$, in terms of a basis of simple harmonic oscillator eigenstates. Tests show that converged results are achieved by including 50 basis functions per mode. In order to assess the validity of the mean-field formulation, we consider second-order perturbation theory corrections to the free energy arising from the subspaces spanned by the soft normal mode directions, but the resulting energies do not change the stability of the structures considered.

The reported anharmonic vibrational energies have been calculated using supercells containing 96 atoms for Pc , $Pna2_1$, $Pca2_1$, and $Pcaa$. The use of non-diagonal supercells means that the results are equivalent to those obtained

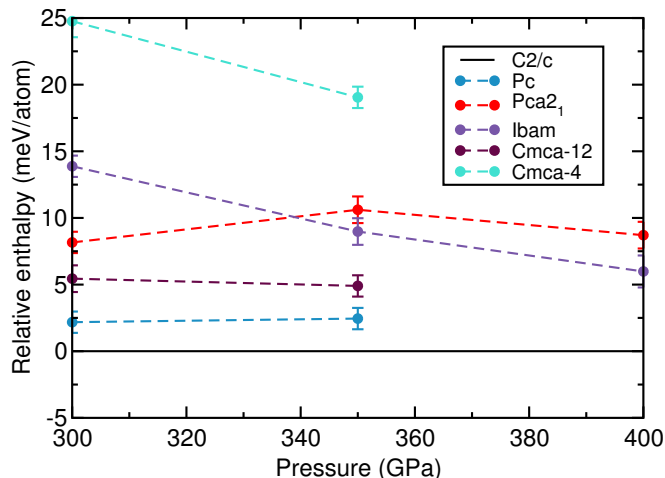


FIG. S2. Relative enthalpies of selected hydrogen structures calculated using DMC. The dashed lines are only a guide to the eye.

with diagonal supercells containing 384 atoms. For $C2/c$ we have used 48-atom cells, equivalent to diagonal supercells containing 192 atoms. For $Cmca$ we have used 36-atom cells, equivalent to diagonal supercells containing 324 atoms, and for $Ibam$ we have used 24-atom cells, equivalent to diagonal supercells containing 216 atoms. Calculations have been performed at pressures from 300 GPa to 450 GPa, in steps of 50 GPa.

QUANTUM MONTE CARLO CALCULATIONS

We have performed selected diffusion Monte Carlo (DMC) calculations [S60] to confirm that the $Pca2_1$ candidate structure is enthalpically competitive. We have used our previously calculated enthalpies for the $C2/c$, Pc , $Cmca-12$, and $Cmca-4$ structures reported in Ref. [S19], and we have performed new calculations for the $Pca2_1$ and $Ibam$ structures. The numerical details of our DMC calculations are the same as those reported in Ref. [S19]. In summary, our calculations are based on the geometries optimised at the PBE level of DFT, noting that using BLYP geometries instead only changes the relative enthalpies by about 1 meV/atom [S19]. We calculate DMC enthalpies using 96-atom cells and the PBE-DFT pressures, and use twist averaging to reduce single-particle errors [S61] and the extrapolation scheme of Kwee, Zhang, and Krakauer (KZK) to reduce long-range interaction errors [S62]. In the KZK scheme, the finite size correction is calculated by comparing standard DFT energies to DFT energies of a modified exchange-correlation functional restricted to a finite sized simulation cell. All DMC calculations have been performed using the CASINO package [S49].

We reproduce the main text figure again as Fig. S2, where we report the relative enthalpies of selected candidate structures of high pressure hydrogen. The results for $C2/c$, Pc , $Cmca-12$, and $Cmca-4$ have already been published in Ref. [S19]. In agreement with these earlier results, we observe that, although $Cmca-12$ and $Cmca-4$ are enthalpically competitive at the DFT level, this is no longer the case at the DMC level. This trend is further exacerbated by the inclusion of vibrational contributions to the energy, thus justifying the neglect of these two structures in the discussion in the main text. We also observe that Pc is energetically competitive with $C2/c$, and as reported in Ref. [S19] it is stabilised by thermal motion. This makes the Pc structure a strong candidate for hydrogen phase IV.

The relative enthalpy of the $Ibam$ structure becomes increasingly competitive with increasing pressure, but remains about 5 meV/atom higher in energy than $C2/c$ at 400 GPa. Furthermore, the vibrational contribution to the energy is significantly larger in $Ibam$ compared to $C2/c$, thus rendering this structure energetically uncompetitive.

The static lattice enthalpy of the $Pca2_1$ structure at the DMC level is higher than that reported in the main text at the DFT level, and is about 9 meV/atom higher than that of $C2/c$ at 400 GPa. However, this difference decreases substantially with the inclusion of the vibrational energy, which at 300 K is 321 meV/atom for $C2/c$ and 313 meV/atom for $Pca2_1$, bringing the relative Gibbs free energy of $Pca2_1$ to only 1 meV/atom above that of $C2/c$. This suggests, in line with our DFT results, that $Pca2_1$ is energetically competitive at the highest pressures. We note that the Pc structure does not exist above about 375 GPa, as it falls into the $Cmca-4$ structure. This observation, together with the relative Gibbs free energies discussed in this section and the results presented in Ref. [S19] suggest

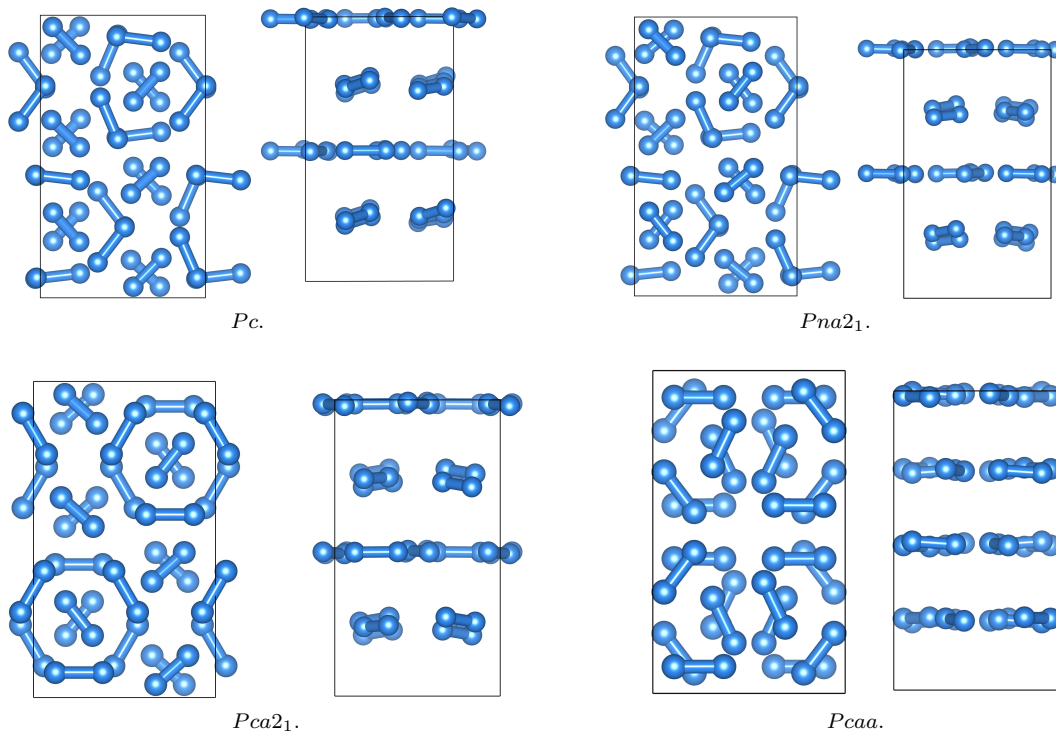


FIG. S3. Top and side views of the Pc , $Pna2_1$, $Pca2_1$, and $Pcaa$ structures.

that Pc is the best candidate for hydrogen phase IV, and $Pca2_1$ is the best candidate for hydrogen phase V. This conclusion is further supported by the comparison of the spectroscopic signatures of the experimental phases and the theoretical structures, as discussed in the main text.

CRYSTAL STRUCTURES

In Fig. S3 we show pictures of the Pc , $Pna2_1$, $Pca2_1$ and $Pcaa$ structures. Their layered nature is most clearly seen from the side view. For Pc , $Pna2_1$, and $Pca2_1$, two types of layers are distinguishable, whereas $Pcaa$ exhibits a unique type of layer.

RAMAN SPECTRA OF MIXED LAYERED STRUCTURES

The Raman spectra reported here and in the main text have been calculated using the PBE density functional [S47]. A comparison of the Raman spectra at 374 GPa of the four most stable mixed structures of high pressure hydrogen, Pc [S13], Cc [S15], $Pna2_1$, and $Pca2_1$, is shown in Fig. S4. The Raman spectra of Pc , Cc , and $Pna2_1$ are almost indistinguishable, and we have used that of the Pc phase in the main text as representative of the Raman spectra of this set of structures.

The $Ibam$ structure is metallic within DFT, and as a consequence we are not able to calculate an accurate Raman intensity profile. However, we can identify the vibrational modes of $Ibam$ that are Raman active by considering the symmetries of the system, and we show the pressure dependence of their frequencies in Fig. S5. As described in the main text, the ν_1 vibron frequency increases with pressure as a consequence of the decrease in bond length in the graphene-like sheets of $Ibam$. This is inconsistent with the experimental data for phase V.

Our searches have found other new structures which, although not energetically competitive with $Pca2_1$ at the static lattice level, have, nonetheless, a relatively low enthalpy. Furthermore, there are other known candidate structures of hydrogen that are also in this regime (not necessarily of orthorhombic symmetry or higher). We have also investigated their Raman spectra, but they are not in agreement with that observed for phase V. The structures investigated have the following space groups: monoclinic ($P2/c$, $C2/c$), orthorhombic ($Pcca$, two variants of $Cmca$, $Cccm$, $Fddd$, and

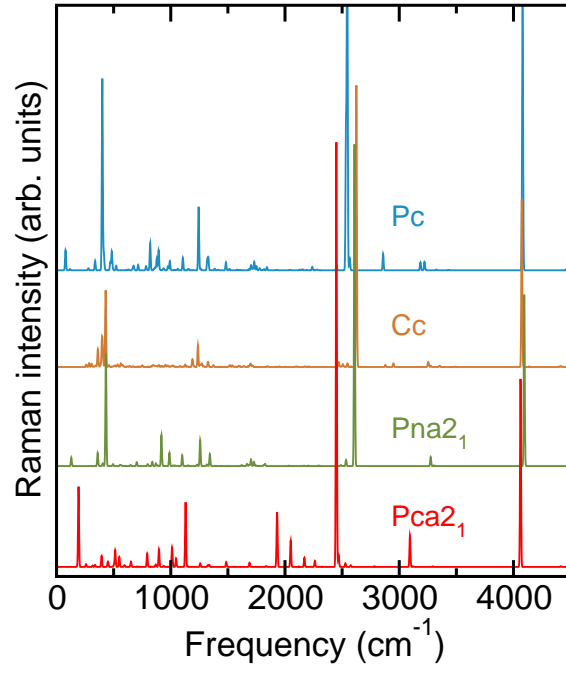


FIG. S4. Raman spectra of Pc , Cc , $Pna2_1$, and $Pca2_1$ at 374 GPa.

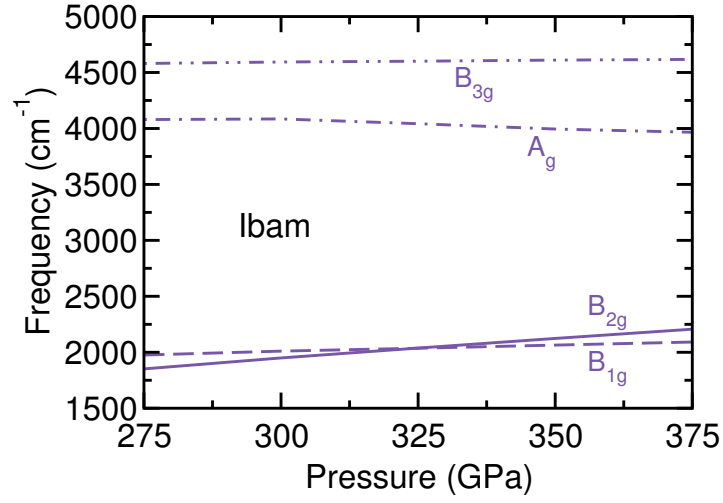


FIG. S5. Pressure dependence of the frequencies of the Raman active modes of $Ibam$.

two additional variants of $Ibam$), tetragonal ($P4_32_12$ and $I4_1/amd$), trigonal ($P3_221$), hexagonal ($P6_3/mmc$), and cubic ($Fd\bar{3}m$).